Nanoscale

RSC Publishing

PAPER

Atomistic modeling of metallic nanowires in silicon†

Cite this: *Nanoscale*, 2013, **5**, 8666

Hoon Ryu,[ae] Sunhee Lee,[be] Bent Weber,[c] Suddhasatta Mahapatra,[c] Lloyd C. L. Hollenberg,[d] Michelle Y. Simmons*[c] and Gerhard Klimeck[e]

Scanning tunneling microscope (STM) lithography has recently demonstrated the ultimate in device scaling with buried, conducting nanowires just a few atoms wide and the realization of single atom transistors, where a single P atom has been placed inside a transistor architecture with atomic precision accuracy. Despite the dimensions of the critical parts of these devices being defined by a small number of P atoms, the device electronic properties are influenced by the surrounding 10^4 to 10^6 Si atoms. Such effects are hard to capture with most modeling approaches, and prior to this work no theory existed that could explore the realistic size of the complete device in which both dopant disorder and placement are important. This work presents a comprehensive study of the electronic and transport properties of ultra-thin (<10 nm wide) monolayer highly P δ-doped Si (Si:P) nanowires in a fully atomistic self-consistent tight-binding approach. This atomistic approach covering large device volumes allows for a systematic study of disorder on the physical properties of the nanowires. Excellent quantitative agreement is observed with recent resistance measurements of STM-patterned nanowires [Weber *et al.*, *Science*, 2012, **335**, 64], confirming the presence of metallic behavior at the scaling limit. At high doping densities the channel resistance is shown to be insensitive to the exact channel dopant placement highlighting their future use as metallic interconnects. This work presents the first theoretical study of Si:P nanowires that are realistically extended and disordered, providing a strong theoretical foundation for the design and understanding of atomic-scale electronics.

Received 10th April 2013
Accepted 2nd July 2013

DOI: 10.1039/c3nr01796f

www.rsc.org/nanoscale

1 Introduction

There has been remarkable progress in the use of a scanning tunneling microscope (STM) to pattern atomic-scale devices in silicon (Si), with the recent demonstration of a single atom transistor,[1] and the presence of Ohmic conduction in highly δ-doped P-monolayer Si (Si:P) nanowires that are just four atoms wide.[2] These two experimental observations show that experimentally the size limit has been reached where dopant placement may become the critical element in the engineering of device properties. Even traditional semiconductor devices that are continually scaled according to the ITRS roadmap have become subject to fluctuations due to atomic-scale effects such as alloy randomness, surface roughness, strain, crystal symmetries, strain, and unintentional doping. In particular the control of dopant placement is critical for the determination of todays transistor performances.[3,4]

Continuous development of STM lithography has enabled precision control of single atom placement with ~5 Å accuracy.[1,5,6] As a result, atomic-precision STM-patterned planar Si:P device architectures have been realized, with a major effort underway to develop a Si-based quantum computer.[1,2,7–9] Here individual donor atoms need to be placed into arrays within a tolerance of the Bohr radius (~25 Å), aligned with nanometer precision to nano-scale control electrodes.[10,11] Within this approach, Si:P nanowires have been proposed as nano-scale interconnects,[9] and have recently been shown to retain Ohmic behavior down to the size of 4 atoms wide.[2] The experimental realization of such Si:P nanowires, however, has raised a variety of interesting and fundamentally important questions that need to be addressed. Atomistic modeling gives us important insights to these questions: (1) "why do such narrow doped nanowires act like a metal?", (2) "what is the spatial extent of the nanowire channels?" and (3) "what is the role of impurity placement fluctuations within the nanowire?". Very limited theoretical understanding has been available so far to address such concerns. More than 15 years ago, Bauer *et al.*,[12] calculated

[a]*National Institute of Supercomputing and Networking, Korea Institute of Science and Technology Information, Daejeon 305-806, Republic of Korea. E-mail: elec1020@gmail.com*

[b]*Samsung Advanced Institute of Technology, Yongin, Gyeonggi-do 446-712, Republic of Korea*

[c]*Centre for Quantum Computation and Communication Technology, School of Physics, University of New South Wales, Sydney, NSW 2052, Australia. E-mail: michelle.simmons@unsw.edu.au; Fax: +61 815 333 2155; Tel: +61 2 9385 6313*

[d]*Centre for Quantum Computation and Communication Technology, School of Physics, University of Melbourne, Parkville, VIC 3010, Australia*

[e]*Network for Computational Nanotechnology, Purdue University, West Lafayette, Indiana 47907, USA*

† Electronic supplementary information (ESI) available. See DOI: 10.1039/c3nr01796f

This journal is © The Royal Society of Chemistry 2013

the equilibrium channel properties of P-doped Si nanowires using an effective mass framework. The approach however used a one-dimensional device description and assumed that the channel was homogeneously doped. More recently, Density Functional Theory (DFT) has been applied to the case of perfectly ordered Si:P nanowires.[13] However, the computational burden of DFT makes it difficult to extend simulations to realistic device sizes to capture the impact of disorder at the atomic-scale, and the consequences for transport in these structures.

In this paper, we answer the questions raised using a fully atomistic $sp^3d^5s^*$ tight-binding (TB) approach and a parallel 3D Schrödinger–Poisson solver that has been developed as an extended functionality of the well-known 3D NanoElectronics Modeling Tool (NEMO-3D).[14] The nearest neighbor TB approach has been previously validated with NEMO-3D simulation projects, especially by modeling the optical energy gap of III–V photodetectors,[15] the valley-splitting in miscut Si quantum wells on SiGe random alloy substrates,[16] the gate-induced stark shift of the hyperfine interaction and quantum confinement created by a single donor in Si Field Effect Transistors (FETs).[17,18] While previous impurity studies with NEMO-3D have focused on modeling quantum confinement due to a single, isolated donor ion in Si FETs,[17,18] this work expands the modeling scope to consider highly doped Si:P nanowires. The equilibrium properties of Si:P devices have been modeled by several groups using a variety of methods, including the single-band effective mass approach,[12] empirical pseudo-potential method assuming parabola subbands,[19] the sp^3s^* TB band model with a set of anti-bonding orbital basis,[20] and DFT.[13,21–23] However, to date all these approaches are limited to the modeling of infinite 2D planar devices,[19–23] or assume uniformly doped channels.[12,13]

This paper extends the modeling approach using a 10-band $sp^3d^5s^*$ TB model coupled with a charge-potential self-consistent calculation. Including the d-orbital basis is critical for a nearest neighbor TB model for describing the electronic structure of Si since the nearest neighbor 5-band sp^3s^* model cannot represent the symmetry of the X valleys.[24] A second nearest neighbor sp^3s^* model is in principle capable of describing the correct symmetries but contains interaction parameters that are neither well controlled nor scalable to heterostructure or impurity interactions. As such the nearest neighbor $sp^3d^5s^*$ offers a compact and accurate model that has been extensively tested and validated.[25,26] This model has been shown to reproduce experimental disorder effects in SiGe/Si miscut quantum wells[16] and impurity states at interface fields.[27] In particular, we focus on simulation results that theoretically substantiate the validity that Ohm's law is maintained in highly doped Si:P nanowires down to the atomic-scale.[2] Our simulation approach is first validated for a 0.25 monolayer (ML) P δ-doped 2D plane (one P atom in every 4 Si atom in the doping plane) at $T = 4.2$ K against previous studies.[19–21] Following this, [110]-oriented 0.25 ML-doped Si:P nanowires that are a single ML thick and 2–8 Si dimer row (DR) (1.5–6.1 nm) wide with an ordered doping profile are the first focal point of this work. Several major findings are reported: (1) metallic behavior is observed and can be explained from the nanowire dispersions, (2) the carrier transport "*via*" donor bands and its confinement to the channel are confirmed by nanowire dispersions and carrier distributions, and (3) the channel doping density and width serve as key control factors of the metallic property of nanowire channels. Finally, Ohmic conduction properties of several highly doped (0.25 ML) ultra-thin Si:P nanowire channels are calculated and compared to recent experiments showing quantitatively excellent agreement.[2] The channel conductance is shown to be insensitive to dopant disorder at a high doping density of 0.25 ML, indicating a strong utility of Si:P nanowires as potential interconnects.

2 Methodology – Si:P device simulations

2.1 Atomistic description of device geometries

Fig. 1(a) depicts the structure of a planar δ-doped Si:P device, which is first simulated to validate our approach through a comparison to previous studies. Since the area of the doping plane in the real device that serves as a 2D electron gas reservoir is usually in the order of 10^6 μm^2,[8] the simulation domain cannot include the entire device due to the computational burden. The device is thus approximated with a supercell that contains 2 donors on a single ML thick Si plane of a (2×4) Si unit-cell area, and an assumption that we have an infinite doping plane with 2D periodic boundary conditions (PBCs) along the plane-parallel directions. The computational cost is therefore dominated by the supercell size along a plane-perpendicular direction, which should be thick enough to represent the Si bulk with a hard-wall boundary condition. At a low temperature of 4.2 K, it is found that the vertical Si spacers around a 2D planar doping δ-layer must extend ~60 ML (8.3 nm) to the top and bottom to avoid any influence of the domain edges on the central doping layer. With a 60 ML buffer of Si, the electron ground state formed by P atoms placed in the middle of the Si box settles within 10^{-5} meV with further increasing Si layer thickness (see the ESI and Fig. S1†). The supercell required to represent a 2D doping plane in the Si bulk,

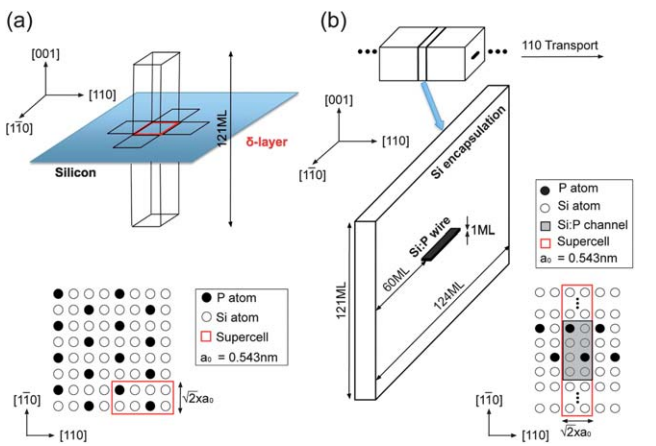

Fig. 1 Simulation domains of 0.25 ML δ-doped Si:P devices: (a) the supercell used to simulate the Si:P 2D δ-layer with an ordered doping profile. (b) The supercell used to describe the Si:P nanowire with an ordered doping profile within the narrow channel.

therefore, has a total of 960 atoms and involves a complex Hamiltonian matrix of 9600 degrees of freedom (DOFs).

Calculations of Si:P nanowires are more demanding than planar doping devices since a narrow Si:P channel is confined laterally by Si layers perpendicular to the transport-orientation. Fig. 1(b) describes the nanowire supercell representing a [110] transport-oriented Si:P nanowire which has a 0.25 ML-doped, 2DR wide channel. The nanowire channel is assumed to be homogeneous such that the nanowire supercell is periodic along the transport direction, and encapsulated by a (120 ML × 120 ML) Si layer to avoid the influence of hard-wall boundaries. (Fig. S2†) As a result the supercell contains a total of 10 240 atoms and a Hamiltonian matrix of 102 400 DOFs. All simulations discussed in this work are performed at a temperature of 4.2 K to compare with experiments. Whilst Fig. 1 only describes Si:P supercells with ordered doping profiles, different supercells were subsequently used to study the effect of dopant disorder and to validate experiments with different dimensions and doping profiles. Corresponding supercells for these simulations are described in the "Results and discussion" section as needed.

In comparison Drumm *et al.*, recently studied Si:P nanowires using DFT which is a remarkable achievement based on the first principle theory.[13] In this work, however, they used a 40 ML thick Si layer and assumed that channels of ordered doping profiles are placed periodically along the transport-perpendicular directions. As a consequence the results are difficult to compare directly with the experimental work,[2] where the dopants in the doping layer are well known to be disordered,[28] and care must be taken to avoid hard-wall boundary effects.

Charge density and potential profiles are calculated self-consistently using a parallel 3D Schrödinger–Poisson solver that has been developed to handle large simulation domains of nanowires. We note that the process for self-consistent simulations and the parallelism adopted for the development, are described in detail in the ESI (Fig. S3 and S4†).

2.2 Electron transport *via* Si:P nanowire channels

Having established the bandstructure and energetic position of the Fermi-level with the Schrödinger–Poisson simulation, the channel conductance at zero source–drain DC bias can be easily calculated in the ballistic regime if the nanowire channel length is comparable to the electron mean-free path, where the flow of electrons will not be significantly affected by scatterings. The model used to calculate the ballistic conductance (G_b) when the supercell is filled with n_e electrons, is shown in eqn (1):

$$G_b(n_e) = \left.\frac{dI_{ds}}{dV_{ds}}\right|_{V_{ds}=0, N=n_e} \simeq \frac{2e^2}{h\Delta V_{ds}} \int_{\beta}^{\alpha} T(\varepsilon)\big(f(\varepsilon) - f(\varepsilon - e\Delta V_{ds})\big)\,d\varepsilon \quad (1)$$

where $\alpha = E_F$, $\beta = E_F - \Delta V_{ds}$, E_F is the Fermi-level energy filling n_e electrons in the nanowire supercell, ΔV_{ds} is the amplitude of a source–drain AC bias variation that is assumed to be $2k_BT$ (~600 μV) throughout in this work. $f(\varepsilon)$ and $T(\varepsilon)$ are the Fermi–Dirac function and the number of sub-bands (modes) at the energy ε, respectively. To simulate charge neutral nanowires, n_e is controlled to be same as the number of P ions placed in nanowire supercells. Since a ballistic approach may not be most appropriate for the simulation of long nanowire channels built experimentally, eqn (1) needs to be modified to incorporate the effect of the impurity scattering as a first order approximation,[29] as shown in eqn (2):

$$G \simeq \frac{\lambda}{\lambda + L_{ch}} G_b \quad (2)$$

where L_{ch} is the channel length, λ is the electron mean-free path and G_b is the channel conductance calculated in the ballistic regime using eqn (1).

3 Results and discussion

3.1 Equilibrium properties of a 2D planar doping Si:P δ-layer

The bandstructure in equilibrium of a 0.25 ML-doped 2D δ-layer is depicted in Fig. 2(a) with a zero energy reference to the Si bulk conduction band minimum (CBM). The infinite doping plane is represented by a supercell with 2D PBCs in real space as illustrated in Fig. 1(a), The k-space dispersion is shown in Fig. 2(a) with 1D cuts along the [110] and [100] direction. Due to the V-shaped potential distribution stemming from the positive impurity ions in the doping plane, the conduction sub-bands are pulled down into the bandgap to ~400 meV below the Si bulk CBM, creating a set of *donor impurity bands*.

The 2D bandstructure has two valleys (marked as 1Γ and 2Γ) at the Γ point ($k = 0$) resulting from the k-space projection of the two Si bulk conduction band ellipsoids that reside along the [001] confinement direction (Fig. 2(b)). The two Γ-valleys exhibit a splitting of ~26 meV, much larger than the valley-splitting calculated for a Si quantum well of same size (~10^{-2} meV). It is well understood that the valley-splitting in confined structures increases as the structural quantization becomes stronger with reduction in physical dimensions.[30,31] The large splitting of Γ-valleys in the 0.25 ML-doped Si:P 2D δ-layer can be thus explained by the strong quantization stemming from the sharply V-shaped impurity potential profile. Four more

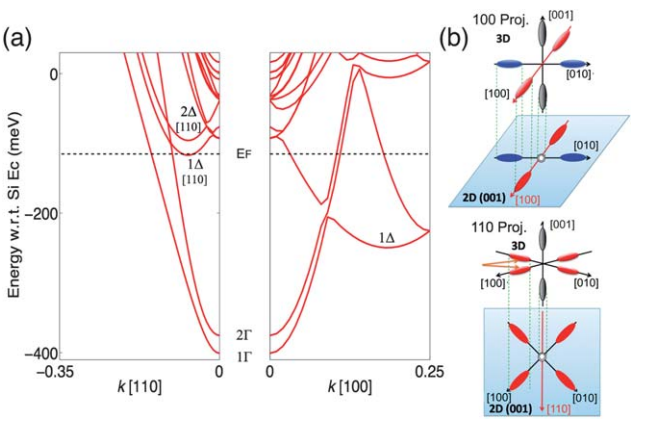

Fig. 2 Bandstructure of the 0.25 ML-doped Si:P 2D δ-layer: (a) the equilibrium bandstructure of a 0.25 ML-doped 2D Si:P δ-layer where the Γ-, Δ-valleys are observed below the Si bulk CBM. (b) 2D projections of the six ellipsoids in the Si bulk conduction band along the [100] and [110] direction.

This journal is © The Royal Society of Chemistry 2013

Table 1 Comparison of calculated dispersions of a 0.25 ML-doped Si:P 2D δ-layer using $sp^3d^5s^*$ tight-binding (this work), empirical pseudopotential (PP), sp^3s^* tight-binding with a set of anti-bonding orbital basis (ABOM), and Density Functional Theory (DFT)

Energy[a]/meV	This work	PP 19	ABOM 20	DFT 21
E_F	−115	−111	−110	−110
1Γ	−401	−410	Not shown	−540
2Γ	−375	−400	Not shown	−420
1Δ	−249	−270	Not shown	−210

[a] All energy values refer the zero energy to the Si bulk CBM.

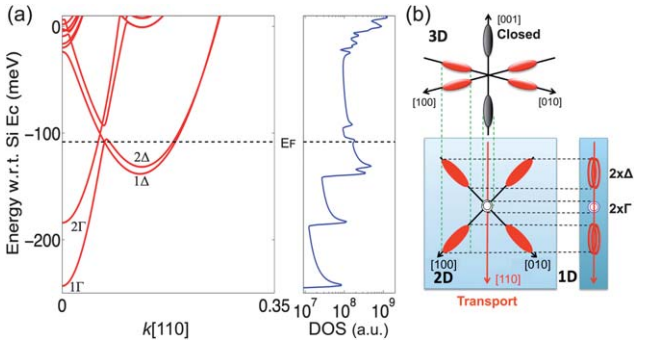

Fig. 3 Bandstructure and DOS profile of the 0.25 ML-doped, 1.5 nm wide Si:P nanowire oriented along the [110] direction: (a) the equilibrium bandstructure and DOS profile of a 0.25 ML-doped, 1.5 nm (2DR) wide [110]-oriented Si:P nanowire. Donor bands are shown below the Si bulk CBM. (b) [110] projection of the six ellipsoids in the Si bulk conduction band.

Δ-valleys result from the four ellipsoids parallel to the (001) plane, but only one of them is shown in the [100] dispersion (marked as 1Δ). The [110] dispersion observes two Δ-valleys (marked as $1\Delta_{[110]}$, $2\Delta_{[110]}$) due to the two ellipsoids residing along the [100] and [010] direction, respectively. Δ-valleys along the [110] direction appear higher in energy than in [100] as the Si bulk CBM happens at 0.185 of the X point.‡

The methodology we have used to determine the equilibrium dispersion of the 0.25 ML-doped Si:P 2D δ-layer can be benchmarked against previous studies for the same system that also assumed ordered doping in the 2D δ-layer as shown in Table 1. Here we can see that the energetic positions of the band minima and the Fermi-level computed with our $sp^3d^5s^*$ TB band model are in an excellent quantitative agreement with results predicted by the empirical pseudopotential method,[19] sp^3s^* TB band model with a set of anti-bonding orbital basis,[20] and DFT approach.[21] The ultimate strength of our method is that it can now consider 2D confined systems such as nanowires, where much larger system sizes are needed to avoid the presence of PBCs. Under these conditions we can now start to study directly the effect of dopant disorder on electronic properties.

3.2 Equilibrium properties of Si:P nanowires

We first calculate the electronic structure of a [110]-oriented, 0.25 ML-doped, 2DR wide Si:P nanowire using an ordered supercell as shown in Fig. 1(b). A total of two electrons are filled in the supercell to place the Fermi-level in charge neutrality. The 1D nanowire dispersion is presented in Fig. 3(a), and corresponding details of the Fermi-level and several valleys of interest are summarized in Table 2 with a zero energy reference to the Si bulk CBM. The donor bands of the nanowire are much closer to the Si bulk CBM compared to the 2D planar doping device (Fig. 2(a)), since the coulomb attraction stemming from the impurity ions becomes weaker due to the narrower doping region. Since the nanowire channel is vertically confined by the surrounding Si bulk layer, the six Si bulk conduction band ellipsoids are projected along the transport direction (Fig. 3(b)) such that a total of two Γ- and two Δ-valleys are observed in the [110] dispersion. The two Γ-valleys show a splitting of ∼60 meV, almost twice that observed in the 2D δ-doping layer, because the 2D confinement in Si:P nanowires results in the stronger quantization of energy levels. The two Δ-valleys are observed at ∼0.13 of the 1st Brillouin zone boundary along the [110] direction.

Table 2 Calculated dispersions and masses of the [110]-oriented, 0.25 ML-doped, 1.5 nm (2DR) wide Si:P nanowire

$sp^3d^5s^*$ TB	Energy[a]/meV	Mass[b]/m_o
E_F	−106	N/A
1Γ	−242	0.16
2Γ	−183	0.22
1Δ	−137	0.58
2Δ	−130	0.59

[a] A zero energy reference to the Si bulk CBM. [b] m_o is the mass of a free-electron.

The dispersion and density of states (DOS) in Fig. 3(a) indicate that the 0.25 ML-doped nanowire channel is metallic, where the Fermi-level intersects a total of six spin-degenerate sub-bands (modes) and sees a non-zero DOS. The DOS profile in Fig. 3(a, right) exhibits a typical distribution of a 1D system that is inversely proportional to the square root of energy with multiple peaks at sub-band minima. The Δ-valleys provide a higher density of electron states than the Γ-valleys because of their heavier masses (close to the effective mass of the Si bulk Δ-valleys) along the [110] direction.§

Fig. 4 illustrates the spatial variations of the electrostatic potential and electron profiles across the nanowire channel. Since the P atoms are placed in an ordered zig-zag pattern as

‡ The absolute values of k vectors used in this work, are all normalized to $2\pi/a_0$, where a_0 is the lattice constant of one Si ⟨100⟩ unit-cell (0.543 nm). The six Δ-valleys in the Si bulk conduction band are experimentally known to be placed at the six $k_{\langle 100\rangle} = (0.84\cdot 2\pi/a_0, 0, 0)$ equivalent points $(0.84\cdot X)$, and are predicted at $0.82\cdot X$ with the empirical $sp^3d^5s^*$ TB model. The 1Δ-valley shows up at $(1 - 0.82)\cdot X = 0.18\cdot X$ in the 1st Brillouin zone of the Si:P supercell in Fig. 1(a) because the 1st Brillouin zone of the supercell expands upto $0.25\cdot X$ due to the reduced zone boundary (zone-folding).

§ The effective mass of the Si bulk Δ-valleys along the [110] direction is ∼0.55 at the room temperature (RT). The Si TB parameters used in this work are fit to the RT mass assuming a negligible change in band curvature at low temperatures.

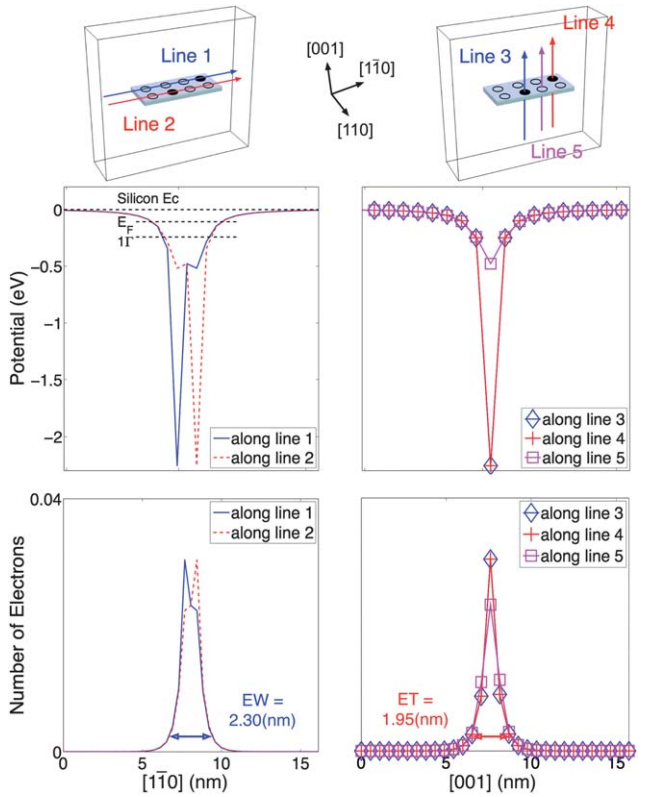

Fig. 4 Potential and electron density profile in the 0.25 ML-doped, 1.5 nm wide [110] Si:P nanowire: potential profile and carrier density are plotted as a function of position along transport and perpendicular directions. Energetic positions of the Fermi-level as well as the 1Γ-valley are indicated in the potential profiles as dashed lines. The effective channel width and thickness are also indicated.

depicted in Fig. 1(b), the 3D data is cut along several lines along the transport-perpendicular directions and the corresponding 1D profiles are provided for a clearer visualization. Carriers are strongly confined to the thin channel due to potential profiles created by P ions, where the core potential on the impurity sites in the channel shows a minimum of −2.26 eV. Tight binding simulations using a $sp^3d^5s^*$ parameter set carried out by Rahman *et al.*,[17] showed that a core potential of −3.78 eV is required to model a single, isolated P ion in the Si bulk to match the ground state energy (45.6 meV below the Si bulk CBM) to experimentally measured values for these systems at low temperature ($T < 4$ K). Interestingly the core potential in the Si:P nanowire (∼−2.2 eV) in Fig. 4 is much higher in energy since the P ions in Si:P nanowires are screened by electrons. Fig. 4 also shows that along the direction vertical to the channel the potential at impurity sites is symmetric and decays rapidly in space. The width of the channel confinement becomes larger along the transverse direction (line 1, 2) than the vertical direction (line 3–5), because the second nearest neighbor impurities along the transverse direction create a wider quantum well than the vertical direction.

While the Si:P channel is lithographically defined to be 2DR (∼1.5 nm) wide and a single ML (∼0.14 nm) thick, the actual electronic width is wider and thicker since the electron wavefunction decays and penetrates into the Si layer. Defining the electronic width of the channel as the point at which the electron density drops to $1/e^2$ of its peak value, we can calculate the effective width and thickness (labeled as EW and ET in Fig. 4) of the 0.25 ML-doped nanowire to be ∼2.30 nm and ∼1.95 nm along the transverse and vertical ([001]) direction, respectively. This indicates that the effective electrostatic channel size is still in an extreme nano-scale regime although the electron charge penetrates into the Si buffer.

3.3 Effects of channel doping profile on Si:P nanowire properties

The effective channel dimensions shown in Fig. 4 clearly support that STM-patterned Si:P nanowires represent a scaling limit of conducting channels. It is, however, easily expected that the electrical properties of the nanowire channels, may be sensitive to variations of the doping profile in the channel. Here, we discuss how the channel doping profiles affect the metallic property of Si:P nanowires, focusing on the doping width and doping density. Effects of dopant disorder within the channel will be discussed separately in the next subsection when we present the results of experimentally measured data.

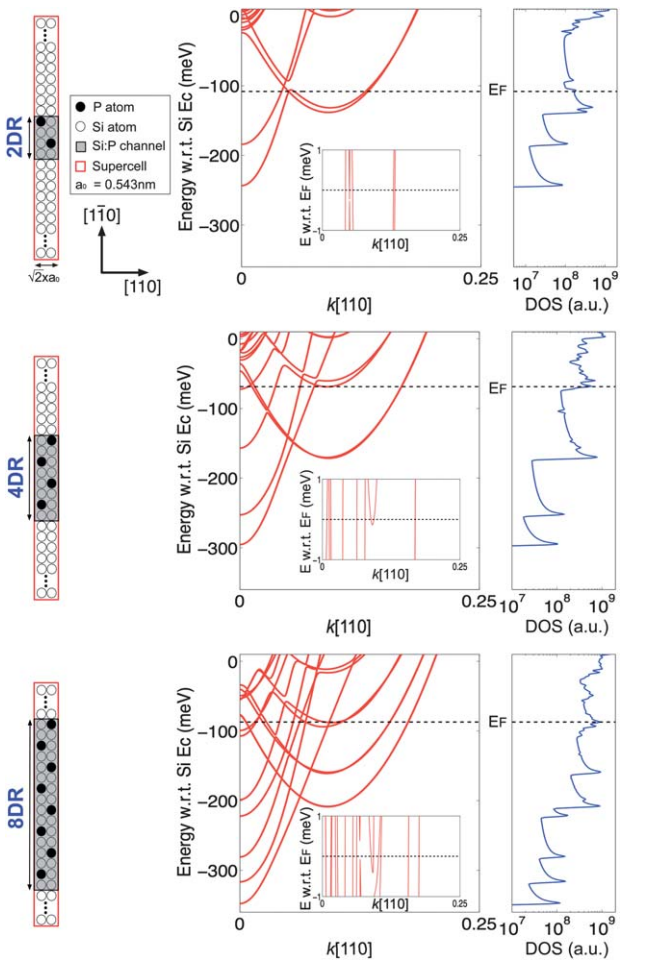

Fig. 5 Dependency of the Si:P nanowire electronic properties on the channel width at a 0.25 ML doping density: nanowire supercells are illustrated with corresponding bandstructures and DOS profiles in equilibrium. Expanded dispersions within 3 k_BT from the Fermi-level are shown in the inset.

This journal is © The Royal Society of Chemistry 2013

Table 3 Comparison of the dispersions between a 2D δ-layer and Si:P nanowires of different widths

Energy[a]/meV	E_F	1Γ	1Δ	$2\Gamma - 1\Gamma$	$E_F - 1\Gamma$
2DRs nanowire	−106	−242	−137	59	136
4DRs nanowire	−69	−295	−170	43	226
8DRs nanowire	−87	−348	−208	31	261
2D δ-layer	−115	−401	−249	26	286

[a] A zero energy reference to the Si bulk CBM.

3.3.1 Channel doping width. The doping width sensitivity is examined by simulating 2DR, 4DR, and 8DR (∼1.5 nm, ∼3.1 nm and ∼6.1 nm, respectively) wide charge-neutral [110] channels with a 0.25 ML doping density. Fig. 5 shows the nanowire supercells, dispersions, and DOS profiles in equilibrium again assuming an ordered doping profile. As the doping width increases from 2DRs to 8DRs, more subbands move below the Fermi-level such that more states are available for conduction. Si:P nanowires becomes more metallic with wider channels since the number of conducting electrons increase. Wider channels contain a larger number of positive donor ions such that the Si bulk conduction sub-bands are pulled down below the Si bulk CBM with stronger coulombic forces, and the donor band minimum thus moves to lower energy. Wider channels also create more donor bands in a denser energy space due to a weaker structural confinement along the transverse direction. The DOS in the Si bulk band-gap increase and its distribution becomes smoother. The ballistic channel conductance will also increase as the nanowires become wider due to more sub-bands crossing the Fermi-level.

Eventually as the doping width increases, the electronic structure of the 0.25 ML-doped Si:P nanowire should resemble that of the 0.25 ML-doped Si:P 2D δ-layer (quantum well). This fact is clearly supported if we consider the summary of nanowires and their comparison with 2D results presented in Table 3. While the Fermi-level itself fluctuates with increasing doping width, its energetic position with respect to the 1Γ-valley ($E_F - E_{1\Gamma} \sim 300$ meV) approaches that of the 2D δ-doped layer. The splitting of the first two Γ-valleys, $E_{2\Gamma} - E_{1\Gamma} \sim 26$ meV also supports this physical phenomenon,¶ approaching that of the 0.25 ML δ-doped layer as the nanowire channel becomes wider. Finally we can see the energetic position of 1Γ-valleys in nanowire dispersions also get closer to that of the 2D δ-doped layer, since the four 1Γ-valleys in the δ-doped 2D layer are projected on [110] direction creating Δ-valleys in the nanowire dispersion (Fig. 3).

3.3.2 Channel doping density. Fig. 6 now considers the impact of the doping density on the electronic properties of Si:P nanowires. Three different doping densities (0.25 (1/4) ML, 0.0625 (1/16) ML and 0.0156 (1/64) ML) are considered for the narrowest, 1.5 nm (2DRs) wide [110] nanowire. Reduction of the channel doping density shifts the donor band minimum (1Γ-valley) closer to the Si bulk CBM and decreases the Γ valley-splitting, as well as the corresponding sub-band quantization due to the reduced channel confinement. The Fermi-level shifts closer to the donor band minimum such that the heavy Δ-valley is completely depleted at a doping density of 0.0156 ML ($\sim 10^{13}$ cm^{-2}). We note the interval of the 1st Brillouin zone is altered for lower doping nanowires as shown in Fig. 6, because a nanowire supercell of a longer channel is needed to simulate the lower doping case.

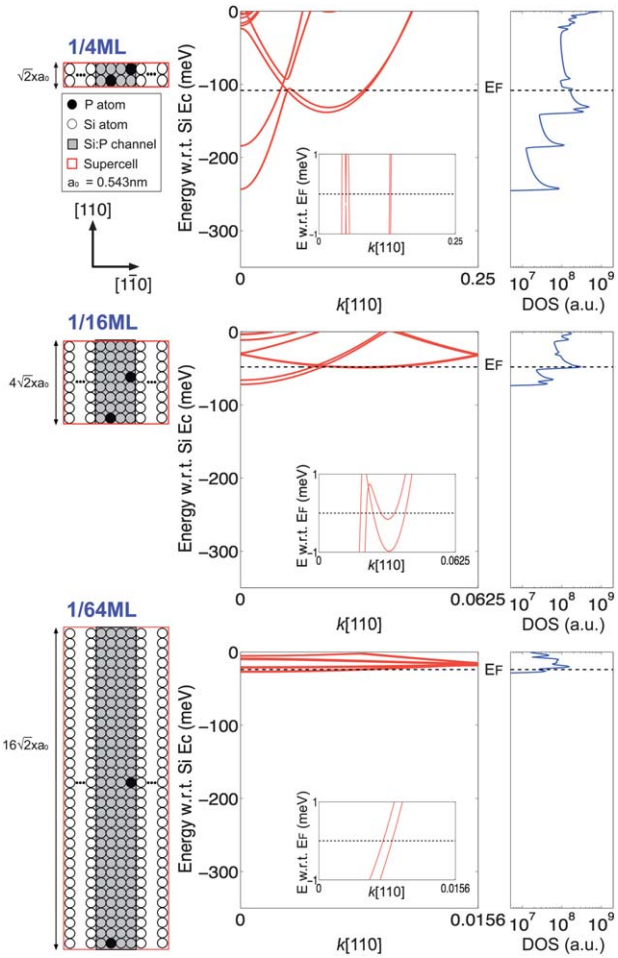

Fig. 6 Dependency of the Si:P nanowire electronic properties on the channel doping density for a 2DR wide nanowires. nanowire supercells are illustrated with corresponding bandstructures and DOS profiles in equilibrium. Expanded dispersions within 3 k_BT from the Fermi-level are shown in the inset.

3.4 Comparison to experimentally measured STM-patterned highly doped Si:P nanowires

Ohmic conduction has recently been observed experimentally in [110] transport-oriented ultra-thin Si:P nanowires, where the channels are 0.25 ML-doped and lithographically patterned to be a few DRs wide using STM-lithography. The channels were embedded in 25 nm epitaxial Si layers to ensure that the

¶ The effective mass of the Si bulk Δ-valleys is heavier along the [001] direction (∼0.92 of the free electron mass) than along the [110] direction (∼0.55 of the free electron mass). So the first two Γ-valleys in nanowire dispersions are formed by the projection of the two Si bulk conduction band ellipsoids on the [001] direction, and the splitting of (1Γ, 2Γ) valleys in nanowires can be thus directly compared to the splitting of (1Γ, 2Γ) valleys of δ-doped 2D layers (quantum wells) that are confined along the [001] direction.

Table 4 Resistance of 0.25 ML-doped [110] Si:P nanowires[2]

Sample	W_c[a]/nm	L_c[b]/nm	$R_{c(E)}$[c]/kΩ	$R_{c(T)}$[d]/kΩ
S1	4.6 (~6DRs)	47	5.2	8.1 ± 1.1
S2	2.3 (~3DRs)	54	10.1	16.3 ± 2.7
S3	2.3 (~3DRs)	20	17.1	7.4 ± 1.2
S4	1.5 (~2DRs)	106	82.3	33.4 ± 4.4

[a] Lithographically defined channel width. [b] Lithographically defined channel length. [c] Channel resistance measured at $T = 4.2$ K. [d] Calculated channel resistance.

electron transport is not affected by the presence of Si surface states.[2] Scattering due to the presence of ionized impurities is however known to play an important role in determining the electronic properties of these highly doped semiconductor devices.[32–34] Goh *et al.* have reported that the electron mean-free path in 0.25 ML-doped Si:P 2D δ-layers is ~8.5 nm at $T = 4.2$ K.[34] Since the electron transport in the four sample nanowires (Table 4) is expected to be significantly affected by elastic scattering along the relatively long channels (>20 nm), we calculated the channel conductance assuming that the mean-free path in 0.25 ML-doped nanowires is comparable to that in the 2D δ-doped layers of the same density. To explore the impact of the dopant placement within the nanowires on the conductance of these highly doped channels, we simulated five different configurations of the channel dopant placement for the same doping density for each nanowire sample S1–S4 (Table 4). The dopant configurations simulated in the nanowire channels are illustrated in Fig. 7.

The set of calculated channel resistances are compared to the experimentally measured results in Fig. 8(a), and in Table 4. Here we present the lithographically defined channel dimensions and experimentally measured resistances for four different Si:P nanowires of different dimensions at $T = 4.2$ K and compare them with our modeling results. As we can see the results give good agreement in both magnitude; and the trend of the conductance with the channel length with deviations occurring at the narrowest nanowires (sample S4†). This is not unexpected since it is likely that for the narrowest channel assuming a 2D mean-free path would not be as valid. Fig. 8(b) and (c) explore the effects of channel dopant disorder on the nanowire DOS. Here we can see that the metallic property of nanowire channels is quite stable at a high doping density of 0.25 ML despite the presence of small fluctuations of the DOS profile. In particular a close up of the DOS at the Fermi-level shown in Fig. 8(c), reveals that despite these fluctuations the DOS remains large with multiple channels to conduct electrons at the Fermi-level. Fig. 8(a) confirms that whilst the channel resistance fluctuates with dopant disorder, the fluctuations are not big enough to drastically break the connection between the modeling and experiment. This is one of the main features of

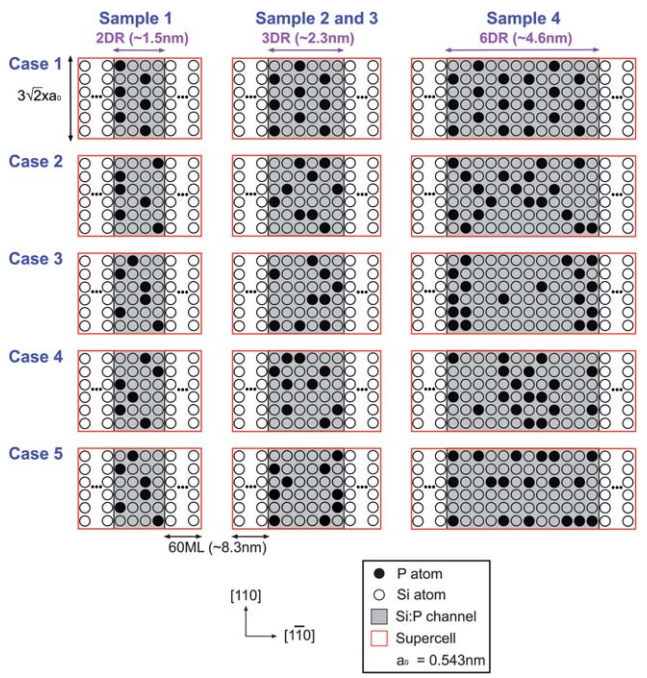

Fig. 7 Doping profiles used in modeling the 0.25 ML-doped Si:P nanowire channels. 5 cases of dopant fluctuations for each NW sample were considered to examine the sensitivity of the channel conductance and DOS profile to the channel dopant placement. Channels are periodic along the transport ([110]) direction, with NW supercells ~2.3 nm long. No consideration was given to longer channel lengths due to the expensive computing cost. Note that Si:P channels are also encapsulated by a 120 ML (~16.6 nm) thick Si layer along the growth ([001]) direction and are assumed to have a doping thickness of a single ML.

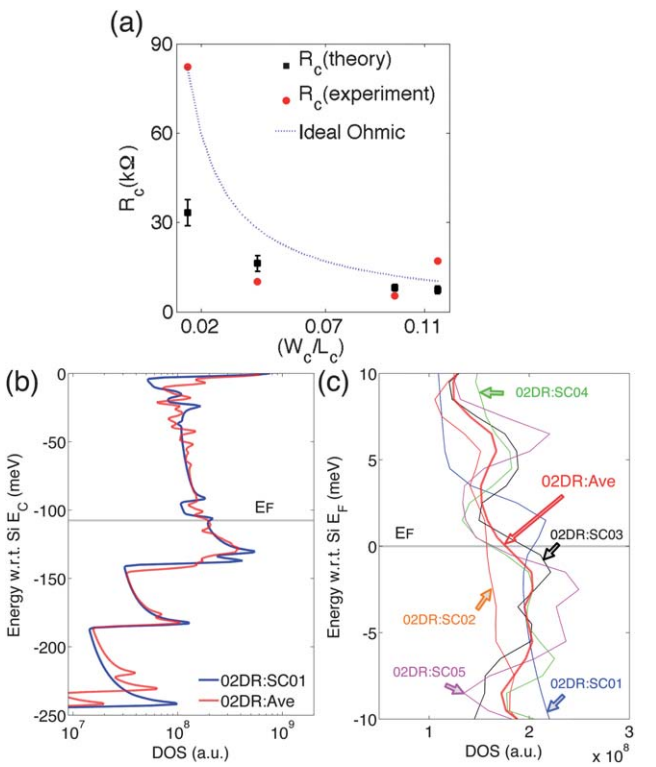

Fig. 8 Resistances and DOS profiles of 2DR Si:P nanowires: (a) measured and calculated channel resistances of four STM-patterned Si:P nanowire samples.[2] (b) Comparison between an ideal 2DR nanowire (Fig. 1(b)) and an average DOS based on the 5 different disordered 2DR nanowire supercells in Fig. 7. (c) A close up of the DOS shown in (b) around the Fermi-level. Fluctuations are observed, but the DOS remains large with multiple channels to conduct electrons at the Fermi-level.

This journal is © The Royal Society of Chemistry 2013

our results – the confirmation that there is a weak sensitivity of the channel conductance to the dopant placement at highly density, $n_s \sim 2 \times 10^{14}$ cm^{-2} (0.25 ML). This result shows that the metallic behavior of these nanowires is stable enough to be considered as potential metallic *interconnects* in atomic-scale devices.

4 Conclusions

We have investigated the electronic structure and transport properties of sub-10 nm wide highly P δ-doped Si (Si:P) nanowires (nanowires) using a 10-band sp^{3}d^{5}s* tight-binding model coupled to 3D Schrödinger–Poisson simulations. The simulation methodology is first validated for a 0.25 ML-doped Si:P 2D δ-layer against previous studies by calculating the energetic position of the Fermi-level, Γ- and Δ-valleys of bandstructures in equilibrium.

Simulation results of a [110]-oriented Si:P nanowire at a 0.25 ML doping density and 1.5 nm width, show that the coulomb attraction stemming from the donor ions is strong enough to create donor bands below the Si bulk conduction band minimum such that the nanowire exhibits metallic behavior even at low temperatures. Critical parameters of the channel doping profile (doping width and doping density) are shown to affect the electrical properties of the nanowires. Increasing the channel width strengthens the metallic property, until the dispersion ultimately resembles that of a 2D δ-doped layer. In contrast, reduction in the channel doping density destroys metallic behavior.

By comparing the calculated channel resistance to the measured data, we not only present a strong connection between the simulations and recent experiments,[2] but also confirm Ohmic conduction of four ultra-thin STM-patterned 0.25 ML-doped [110] Si:P nanowires that are physically realized. The insensitivity of the channel resistance in highly doped 0.25 ML nanowires to the channel dopant disorder is demonstrated by simulating a large number of nanowire supercells. The demonstration that metallic behavior in these highly doped nanowires is insensitive to the dopant placement bode well for the utility of highly doped Si:P nanowires as ultrathin metallic interconnects for atomic-scale devices.

Acknowledgements

This research was conducted by the http://www.nanoHUB.org computing resources operated by the Network for Computational Nanotechnology funded by the US National Science Foundation (NSF) (EEC-0228390), and the financial support from the US NSF (OCI-0749140), the US Army Research Office (W911NF-08-1-0527), and the Australian Research Council (ARC) Centre of Excellence for Quantum Computation and Communication Technology (CE11 0001027). H. Ryu, S. Lee and G. Klimeck acknowledge the extensive use of computing resources provided by the TeraGrid computing resources supported by the National Institute for Computational Sciences, and the Texas Advanced Computing Center. H. Ryu acknowledges the extensive use of TACHYON-II clusters supported by the National Institute of Supercomputing and Networking, Korea Institute of Science and Technology Information, and the support from the EDucation-research Integration through Simulation On the Net (EDISON) project funded by the Ministry of Education, Science and Technology, Republic of Korea (Grant no.: 2011-0020576). M. Y. Simmons acknowledges an ARC Federation Fellowship and support from the US Semiconductor Research Corporation.

References

1 M. Füchsle, J. A. Miwa, S. Mahapatra, H. Ryu, S. Lee, O. Warschkow, L. C. L. Hollenberg, G. Klimeck and M. Y. Simmons, *Nat. Nanotechnol.*, 2012, **7**, 242–246.
2 B. Weber, S. Mahapatra, H. Ryu, S. Lee, A. Fuhrer, T. C. G. Reusch, D. L. Thompson, W. C. T. Lee, G. Klimeck, L. C. L. Hollenberg and M. Y. Simmons, *Science*, 2012, **335**, 64–67.
3 T. Shinada, S. Okamoto, T. Kobayashi and I. Ohdomari, *Nature*, 2005, **437**, 1128–1131.
4 A. Martinez, N. Seoane, A. R. Brown, J. R. B. Barker and A. Asenov, *IEEE Transactions on Nanotechnology*, 2009, **8**, 603–610.
5 S. R. Schofield, N. J. Curson, M. Y. Simmons, F. J. Ruess, T. Hallam, L. Oberbeck and R. G. Clark, *Phys. Rev. Lett.*, 2003, **91**, 136104.
6 F. J. Ruess, L. Oberbeck, M. Y. Simmons, K. E. J. Goh, A. R. Hamilton, T. Hallam, S. R. Schofield, N. J. Curson and R. G. Clark, *Nano Lett.*, 2004, **4**, 1969–1973.
7 A. Fuhrer, M. Füchsle, T. C. G. Reusch, B. Weber and M. Y. Simmons, *Nano Lett.*, 2009, **9**, 707–710.
8 F. J. Ruess, W. Pok, K. E. J. Goh, A. R. Hamilton and M. Y. Simmons, *Phys. Rev. B: Condens. Matter Mater. Phys.*, 2007, **75**, 121303.
9 F. J. Ruess, B. Weber, K. E. J. Goh, O. Klochan, A. R. Hamilton and M. Y. Simmons, *Phys. Rev. B: Condens. Matter Mater. Phys.*, 2007, **76**, 085403.
10 B. E. Kane, *Nature*, 1998, **393**, 133–137.
11 L. C. L. Hollenberg, A. D. Greentree, A. G. Fowler and C. J. Wellard, *Phys. Rev. B: Condens. Matter Mater. Phys.*, 2006, **74**, 045311.
12 G. E. W. Bauer, *Phys. Rev. B: Condens. Matter Mater. Phys.*, 1991, **43**, 4023.
13 D. W. Drumm, J. S. Smith, M. C. Per, A. Budi, L. C. L. Hollenberg and S. P. Russo, *Phys. Rev. Lett.*, 2013, **110**, 126802.
14 G. Klimeck, S. S. Ahmed, H. Bae, N. K. R. R. S. Clark, B. Haley, S. Lee, M. Naumov, H. Ryu, F. Saied, M. Prada, M. Korkusinski and T. B. Boykin, *IEEE Trans. Electron Devices*, 2007, **54**, 2079–2089.
15 M. Usman, H. Ryu, I. Woo, D. S. Ebert and G. Klimeck, *IEEE Transactions on Nanotechnology*, 2009, **8**, 330–344.
16 N. Kharche, M. Prada, T. B. Boykin and G. Klimeck, *Appl. Phys. Lett.*, 2007, **90**, 092109.
17 R. Rahman, C. J. Wellard, F. R. Bradbury, M. Prada, J. H. Cole, G. Klimeck and L. C. L. Hollenberg, *Phys. Rev. Lett.*, 2007, **99**, 036403.

18 G. P. Lansbergen, R. Rahman, C. J. Wellard, I. Woo, J. Caro, N. Collaert, S. Biesemans, G. Klimeck, L. C. L. Hollenberg and S. Rogge, *Nat. Phys.*, 2008, **4**, 656–661.
19 G. Qian, Y.-C. Chang and J. R. Tucker, *Phys. Rev. B: Condens. Matter Mater. Phys.*, 2005, **71**, 045309.
20 X. Cartoixà and Y. C. Chang, *Phys. Rev. B: Condens. Matter Mater. Phys.*, 2005, **72**, 125330.
21 D. J. Carter, O. Warschkow, N. A. Marks and D. R. McKenzi, *Phys. Rev. B: Condens. Matter Mater. Phys.*, 2009, **79**, 033204.
22 D. J. Carter, N. A. Marks, O. Warschkow and D. R. McKenzie, *Nanotechnology*, 2011, **22**, 1–10.
23 D. Drum, A. Budi, M. Per, S. Russo and L. C. L. Hollenberg, *Nanoscale Res. Lett.*, 2013, **9**, 111.
24 G. Klimeck, R. C. Bowen, T. B. Boykin, C. Salazar-Lazaro, T. A. Cwik and A. Stoica, *Superlattices Microstruct.*, 2000, **27**, 77–88.
25 G. Klimeck, F. Oyafuso, T. Boykin, R. Bowen and P. Allmen, *Comput. Model. Eng. Sci.*, 2002, **3**, 601–642.
26 J. Wang, A. Rahman, A. Ghosh, G. Klimeck and M. Lundstrom, *Appl. Phys. Lett.*, 2005, **86**, 093113.
27 R. Rahman, G. Lansbergen, S. Park, J. Verduijn, G. Klimeck, S. Rogge and L. Hollenberg, *Phys. Rev. B: Condens. Matter Mater. Phys.*, 2009, **80**, 098936.
28 G. Scappucci, W. M. Klesse, A. R. Hamilton, G. Capellini, D. L. Jaeger, M. R. Bischof, R. F. Reidy, B. P. Gorman and M. Y. Simmons, *Nano Lett.*, 2012, **12**, 4953–4959.
29 S. Datta, F. Assad and M. S. Lundstrom, *Superlattices Microstruct.*, 1998, **23**, 771–780.
30 N. Neophytou, A. Paul, M. S. Lundstrom and G. Klimeck, *IEEE Trans. Electron Devices*, 2008, **55**, 1286–1297.
31 S. Goswami, K. A. Slinker, M. Friesen, L. M. McGuire, J. L. Truitt, C. Tahan, L. J. Klein, O. J. Chu, P. M. Mooney, D. W. van der Weide, R. R. Joynt, S. N. Coppersmith and M. A. Eriksson, *Nat. Phys.*, 2007, **3**, 41–45.
32 E. Conwell and W. F. Weisskopf, *Phys. Rev.*, 1950, **77**, 388–390.
33 N. L. Mattey, T. E. Whall, R. A. Kubiak and M. J. Kearney, *Semicond. Sci. Technol.*, 1992, **7**, 604–607.
34 K. E. J. Goh, L. Oberbeck, M. Y. Simmons, A. R. Hamilton and M. J. Butcher, *Phys. Rev. B: Condens. Matter Mater. Phys.*, 2006, **73**, 035401.

 This journal is © The Royal Society of Chemistry 2013